Advances in Potential Formation and Findings in Sheared Radial Electric-Field Effects on Turbulence and Loss Suppression in GAMMA 10

T. Cho, H. Higaki, M. Hirata, H. Hojo, M. Ichimura, K. Ishii, M. K. Islam, A. Itakura, I. Katanuma, J. Kohagura, Y. Nakashima, T. Numakura, T. Saito, Y. Tatematsu, M. Yoshikawa, M. Yoshida, T. Imai, V. P. Pastukhov*, and S. Miyoshi

Plasma Research Centre, University of Tsukuba, Tsukuba, Ibaraki 305-8577, Japan

E-mail: tcho@prc.tsukuba.ac.jp

Abstract. Following the Lyon IAEA Conference, (1) ***a factor of three progress*** up to 2.1 kV in the formation *of ion-confining potential heights* in comparison to those attained 1992-2002 is achieved for tandem-mirror plasmas in the hot-ion mode with ion temperatures of several keV. (2) The advance in the potential formation gives bases for a *finding of the remarkable effects of radially produced shear of electric fields* E_r, *or non-uniform sheared plasma rotation* $\omega_r = E_r/(r_cB)$ *on the suppression of turbulent fluctuations* for the first time in GAMMA 10. (Here, r_c denotes a radius mapped to the central-cell.) (2-i) Such a shear effect on the central-cell plasmas is highlighted visually by x-ray tomography diagnostics; that is, spatially and temporally ***fluctuated vortex-like structures are clearly observed*** in plasmas produced by ICH alone [having a quite ***weak shear***]. (2-ii) However, during the application of plug ECH into the ICH plasmas, an associated potential rise produces a ***stronger shear*** [E_r=several 10 kV/m^2]. In this case, ***the disappearance of the turbulent vortices*** on the basis of such a high-potential formation due to ECH is found in association with ***plasma confinement improvement***. In fact, *the associated temperature rise and transverse loss suppression are observed*. (3) From the viewpoints of both (i) a *conventional* idea of higher and *better potential confinement in the axial direction* [i.e., E_z effects] and (ii) the present ***new finding of a turbulent vortex disappearance due to a strong radial electric shear*** [i.e., E_r effects] *in the transverse direction*, simultaneously, such a high potential formation is found to play an essential role in providing stably improved plasma confinement both radially and axially. (4) *For the physics interpretations and control of such potential* [or the associated E_r or ω_r shear] formation, the validity of our proposed theory of the potential formation is extendedly tested under the conditions with auxiliary heatings. The ***data described above well fit to the extended surfaces calculated from our proposed consolidated theory*** of the strong ECH theory (plateau formation) with Pastukhov's theory on energy confinement. The validity of the extension of our proposed physics mechanism encourages the future extendable scalability of potential formation having prospective *simultaneous* E_z *and* E_r *(or* ω_r*) shear effects on confinement improvements*.

1. Introduction

Experimental verification of the effects of the formation of radially sheared electric fields E_r (or potentials) in plasmas is one of the most critical issues to understand physics bases for plasma-confinement improvements, which have been found in various types of devices including tokamaks and helical devices. One of the most essential and inherent characteristic *advantages of open-ended mirror devices* [1-8] is the *ease of control of a radial potential distribution and the associated* E_r *shear profile* or the frequency of a non-uniform (or sheared) plasma rotation [$\omega_r=E_r/(r_cB)$] profile. Such a control of E_r or ω_r in mirror devices is easily carried out on the basis of driving axial fast electron flows from plug electron-cyclotron heating (ECH) regions [8] into *open-ended* mirror regions along the lines of magnetic force [8-12]. (Here, r_c denotes a radius mapped to the central-cell.) Thus, the profile control of the axial electron flows due to ECH power control of the radial distribution and intensity (see below) provides a convenient "active control" method of the radial shear profile. This allows for flexible and characteristic mirror experiments to construct common relations between the shear profiles and reductions in plasma fluctuation-driven radial losses (or transverse confinement) together with physics details of interior hot-plasma behavior, as described below.

2. Experimental Apparatus

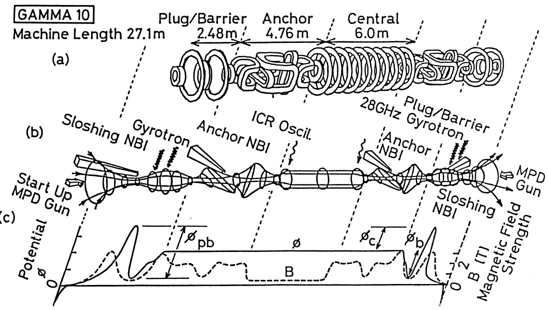

FIG. 1. *Schematic view of the GAMMA 10 tandem-mirror; (a) magnetic coil set, (b) magnetic-flux tube with heating systems, as well as (c) axial magnetic-field (dashed curve) and potential profiles (solid curve).*

GAMMA 10 is a minimum-*B* anchored tandem mirror with outboard axisymmetric plug and barrier cells [5,13-15]. It has an axial length of 27 m, and the total volume of the vacuum vessel is 150 m^3 (Fig. 1). The central cell has a length of 6 m and a fixed limiter with a diameter of 0.36 m, and the magnetic-field intensity at the midplane B_z=B_m is 0.405 T with a mirror ratio R_m of 5.2. Ion-cyclotron heatings (ICH) (200 kW at 4.47 or 6.36 MHz, as well as 100 kW at 9.9 or 10.3 MHz) are employed for the central-cell hot-ion production and the anchor stabilization, respectively [16-18]. The plug and barrier cells are axisymmetric mirrors; they have an axial length of 2.5 m (B_m=0.497 T, and R_m=6.2). Microwaves at 28 GHz are injected in the extraordinary mode into the plug and the barrier regions [8,9,16] to produce an ion-confining potential ϕ_c, and a thermal-barrier potential ϕ_b, respectively.

Plug potentials ϕ_P are measured with originally developed electrostatic spectrometer arrays (IES) [19] for end-loss-ion energy analyses. Central-cell potentials ϕ_C and barrier potentials ϕ_B are directly measured with heavy-ion (Au^0) beam probes (HIBP) [20]. Therefore, one can obtain ϕ_c and ϕ_b, as ϕ_P-ϕ_C and ϕ_C-ϕ_B, respectively.

3. Three-Times Progress in Ion-Confining Potential ϕ_c Formation as Compared to That Attained 1992-2002

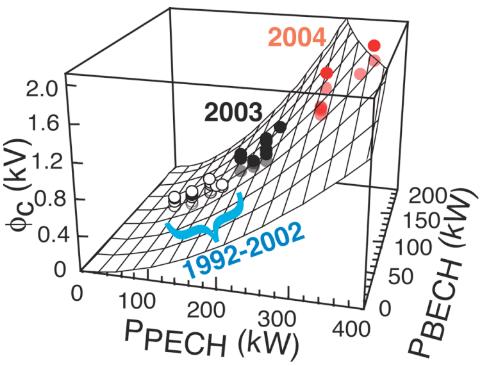

FIG. 2. *After the IAEA 2002 (Lyon), three-times advance in ion-confining potential (ϕ_c) formation including a record of 2.1 kV (filled circles), in comparison to ϕ_c attained 1992-2002 (open circles), is achieved. These extended data fit well to the scaling surface of ϕ_c with plug (P_{PECH}) and barrier (P_{BECH}) ECH powers (see Refs. [13], and [14]). Here, a tandem mirror potential configuration with n_p/n_c=0.1 having T_i=several keV is employed.*

Recently, *three-times progress* in the formation of ϕ_c including *a new record of 2.1 kV* in the plug region (filled circles in Fig. 2), in comparison to ϕ_c attained 1992-2002 [13,14] (open circles in Fig. 2), is achieved in a hot-ion mode [13-17] having bulk-ion temperatures T_i=several keV. The advance in the potential formation leads to a finding of remarkable effects of *sheared* E_r ($E_r' \equiv dE_r/dr_c \approx$several 10 kV/$m^2$) *or sheared* ω_r (i.e., $\omega_r' \equiv d\omega_r/dr_c$) on the suppression of both coherent drift-wave-like spectral component and broad-band turbulent fluctuations (or vortex-like structures; see below) in GAMMA 10. Here, the progress in the potential formation is made in line with the extension of our proposed scaling of ϕ_c with powers of plug (P_{PECH}) and barrier ECH (P_{BECH}) [13,14] (see the data fit to the scaling surface in Fig. 2) covering representative tandem-mirror operational modes, characterized in terms of a high-potential mode having kV-order plasma-confining potentials [5,8] and a hot-ion mode yielding fusion neutrons with T_i=10-20 keV [16].

4. Observations of Remarkable Effects of Radially Sheared Electric Fields Produced by High Potential Formation on the Suppression of Turbulent Fluctuations

The progress of higher ϕ_c formation in turn gives bases for the following remarkable effects of the formation of a strong central-cell E_r *or* Ω_r *shear*, since *the shear* is proportional to the central-cell (ϕ_C) and plug potentials (ϕ_P). Along the lines of magnetic force, ϕ_C is closely connected with and raised by a ϕ_P rise due to plug ECH having the Gaussian power-lobe profile of $P_{ECH}(0)(\exp[-(r_c/a)^2])$. In fact, such a proportionality of $\phi_C(r_c)$ to $\phi_P(r_c)$ is experimentally observed [10,11]. Here, $\phi_C(0)$ and $P_{ECH}(0)$ designate the values at r_c=0.

Non-uniform plasma rotation can suppress existing plasma instabilities and fluctuations. As a result, the considerable reduction of cross-field plasma transport is expected. According to a review paper [21], the stability of rotating plasmas is similar to the stability of rotating stratified fluids and depends on profiles of Ω_r and densities n. For the plasmas with non-uniform density profiles the most general and invariant measure of the velocity shear effects is the vorticity of plasma momentum density or, briefly, "dynamic vorticity" $\boldsymbol{W}=(\nabla\times n\boldsymbol{V}_E)$. In our case of the axisymmetric plasma rotation, the z-component of $\boldsymbol{W}$ normalized to the unit density at r_c=0 (i.e., $W_r=[\nabla\times(n\boldsymbol{V}_E)]_z/n(0)=(nr_c^2\Omega_r)\partial[n(0)r_c])$ is the most appropriate measure of the $\boldsymbol{E}\times\boldsymbol{B}$ velocity ($\boldsymbol{V}_E$) shear. The W_r value directly relates to the E_r shear and is a natural generalization of the velocity shear parameter, which is well-known for slab flows with a uniform density [$W_{slab\text{-}x}=dV_E/dx$]. Further, even in the cylindrical geometry, when n and ϕ_c have the Gaussian profiles with the same e-folding lengths, the W value is described as $W_r=(2/B)[n/n(0)](dE_r/dr)$.

In Fig. 3(a), the central-cell line density nl_c of a hot-ion mode plasma with T_i=4 keV increases during plug ECH in association with reducing fluctuations. Fluctuation diagnostics including a movable microwave interferometer, the Fraunhofer-diffraction method [22], two sets of our developed fifty-channel soft x-ray detectors using microchannel plates (MCP) [8,9,23] in the central-cell midplane, eight Langmuir probes (i.e., every 45° at r_c=18 cm in the central cell) for wave phasing and coherence diagnostics [18], the above described HIBP [20] and eight sets of IES [19], and simultaneous potential diagnostics with HIBP and IES, show consistently the same characteristic features as described below.

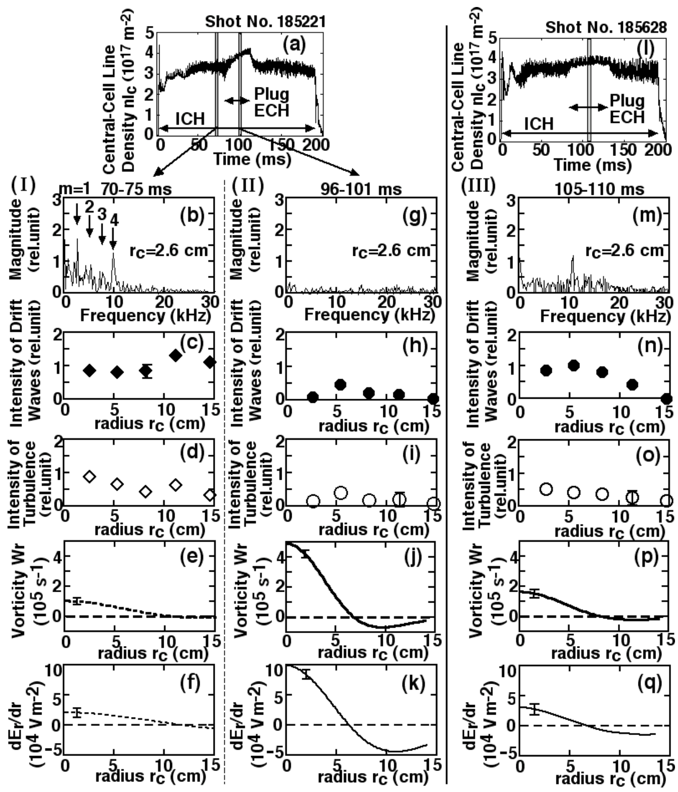

FIG. 3 Data sets of (I) ICH plasmas with a low W_r or a weak shear [(b)-(f)], and (II) with plug ECH (180 kW) producing a strong shear [(g)-(k)]. In (b), Fourier component of coherent drift-like waves with mode numbers m and low-frequency broad-band (continuous) incoherent turbulent signals for IES, for instance, are suppressed in (g)-(k) except around $r_c\approx$ 6-7 cm having ≈zero dynamic vorticity W_r or no E_r shear [(j) or (k)]. (III) Another data set during lower plug ECH (120 kW) in (m)-(q) having a weaker shear as compared to that in (g)-(k). Noisier and earlier-saturated density rise in (l) during ECH is found in comparison to that in (a).

At first, two data sets, one before [Figs. 3(b)-3(f)] and one during ECH [Figs. 3(g)-3(k)] (P_{ECH} =180 kW), are compared. Frequency analyses of IES signals, for instance, are shown in Fig. 3(b). The existence of electron drift-wave-like spectral components with the mode numbers m=1, 2, etc. [18,22], giving peaked structure (see arrows) over a few kHz [22], and *turbulent fluctuations* having *incoherent azimuthal phase relation* and *broad-band frequency spectrum* are found. In Figs. 3(c) and 3(d), the frequency-integrated intensities of the drift-like waves and the turbulent fluctuations are plotted at several r_c, respectively. In Figs. 3(e) and 3(j), W_r deduced from measurements of the density profile and $\square_C$ with IES [19] and HIBP is plotted. It is found that a low W_r (weak shear) is formed in the case without ECH [Fig. 3(e)]. On the other hand, a data set during ECH [Figs. 3(g)-3(k)] having a higher W_r (stronger shear) [Fig. 3(j)] shows a significant difference. Figures 3(h) and 3(i) show a considerable reduction of fluctuations over all radii and particularly near the plasma axis and $r_c \approx 10$ *cm*, where $\square W_r \square$has the maximum values. Nevertheless, an appreciable level of fluctuations still exists around $r_c \approx$ *6-7 cm*, where $W_r \approx 0$. In Figs. 3(f), 3(k), and 3(q), dE_r/dr_c is also plotted as a measure of the E_r shear; these reflect the above-described relation between the vorticity W_r and dE_r/dr_c.

In Figs. 3(m)-3(q), a similar data set to that in Figs. 3(b)-3(f) having turbulent is obtained, although ECH (P_{ECH} =120 kW) is applied in Figs. 3(m)-3(q) as in Figs. 3(g)-3(k). However, remarkably different behavior is found in these two data sets. As one can see in Fig. 3(p), a weaker shear than that in Fig. 3(j) is formed. For this weak shear, a lower-level saturation of density rise is found during ECH [Fig. 3(l)] with stronger density fluctuations [see and compare nl_c in Fig. 3(a) during ECH].

5. The Radially Formed Shear Effects on Improvements in Plasma Confinement

The difference in the density rise in Figs. 3(a) and 3(l) is carefully investigated by the use of a widely employed particle-balance equation of $edN/dt=I_s-I_{//}-I_{\square}$ [1,4,5,8,11,22]. Here, the contribution of nonambipolar $I_{\square}$ to total $I_{\square}$ is observed to be ignorable as compared to ambipolar $I_{\square}$ by using floated end plates having ≈M□ resistance as a “net current detector” array (for more details, see Ref. [24] for the nonambipolar $I_{\square}$ suppression) even for the case in Figs. 3(a)-3(q).

In Fig. 4(a), a rising rate edN/dt of the total particle number N during ECH [see Fig. 3(a)] integrated along a specific axial flux tube well balances the difference between particle source currents I_s deduced from $H_{\square}$ detector-array data and an axial loss currents $I_{//}$ from IES placed along the corresponding flux tube (for more detail, see Refs. [1], [5], [11], and [22]). It is noted that $I_{//}$ is obtained from the envelop of “sawtoothed” end-loss signals in Fig. 4(b) because of a sinusoidal ion-repeller biasing for IES [19]. This shows negligible transverse particle losses $I_{\square}$. The property of $I_{//}>>I_{\square}$ is consistently confirmed by good agreement between the data on $I_{//}$ in Fig. 4(b) and Pastukhov’s theoretically evaluated $I_{//}$ [filled circles in Fig. 4(b)], since the Pastukhov theory [7] predicts $I_{//}$ under the assumption of negligible $I_{\square}$.

On the other hand, the data in Figs. 4(d) and 4(e) correspond to the data set in Figs. 3(l)-3(q). By the use of the same methods, an appreciable amount of $I_{\square}$ [see diamonds in Fig. 4(d) during ECH, as compared with those in Fig. 4(a) during ECH] is found; for instance, $I_{\square} \approx (1/2) I_{//}$ at t=100 ms in Fig. 4(d). It is also noted that $I_{//}$ observed at t=100 ms in Fig. 4(e) ranges consistently around 2/3 of Pastukhov’s predicted $I_{//}$. The remainder part of 1/3 of the predicted $I_{//}$ is interpreted in terms of the existence of the radially directed losses $I_{\square}$ before the axial-loss currents reach mirror-end regions.

This is consistent with the fact of an earlier saturation of nl_c in Fig. 3(l) with a weak shear in comparison to its continuous rise in Fig. 3(a) during ECH with a strong shear. Similar behavior is also found before ECH [at t=75 ms in Fig. 3(a)], when a weak shear is formed with turbulent signals [Figs. 3(b)-3(f)]. Again, the particle balance requires an appreciable $I_\perp$ [Fig. 4(a)], and disagreement between anticipated $I_{//}$ and the data on $I_{//}$ in Fig. 4(b) is consistently observed.

In line with the above-described discussions, the theoretical particle-balance procedure is applied to fit to the data on nl_c in Figs. 4(c) and 4(f) with the information on no appreciable changes in density profiles during ECH. The data on nl_c are well traced by the particle-balance-analyzed solid curves [Figs. 4(c) and 4(f)] with the on-axis total particle-confinement time τ_{total}=75 ms [i.e., $\tau_{//}$=95 ms, $\tau_\perp$>4 $\tau_{//}$, and ϕ_c=0.84 kV at t=100 ms in Fig. 4(c) with a *strong shear* in Fig. 3(j); Pastukhov's ion-energy-confinement time τ_E=50 ms for the *present medium height* of ϕ_c=0.84 kV in the hot-ion mode], while τ_{total}=28 ms [i.e., $\tau_{//}$=45 ms, and $\tau_\perp$=90 ms for *lower* ϕ_c=0.48 kV at t=100 ms in Fig. 4(f) with a *weak shear* in Fig. 3(p)].

On the other hand, Pastukhov's theoretical particle-confinement time τ_{Pastu}=96 ms in Figs. 4(c) agrees well with the above experimentally obtained $\tau_{//}$ under the condition of $\tau_\perp$>>$\tau_{//}$. In Fig. 4(f), τ_{Pastu}=28 ms well interprets the experimental values of $\tau_{//}$=45 ms, and $\tau_\perp$=90 ms, since the observed $\tau_{//}$ should increase if $I_\perp$ becomes ignorable. Here, from the fact that $I_\perp$≈(1/2) $I_{//}$ at t=100 ms in Fig. 4(c), if one assumes negligible $I_\perp$, then the additional amount of $I_\perp$ flows into the end regions as an additional $I_{//}$. As a result, $I_{//}$ increases by 3/2, giving a modified $\tau_{//}$=45/(3/2) ms=30 ms. This value should be consistent with τ_{Pastu}=28 ms, since Pastukhov's theory is valid under the assumption of negligible $I_\perp$.

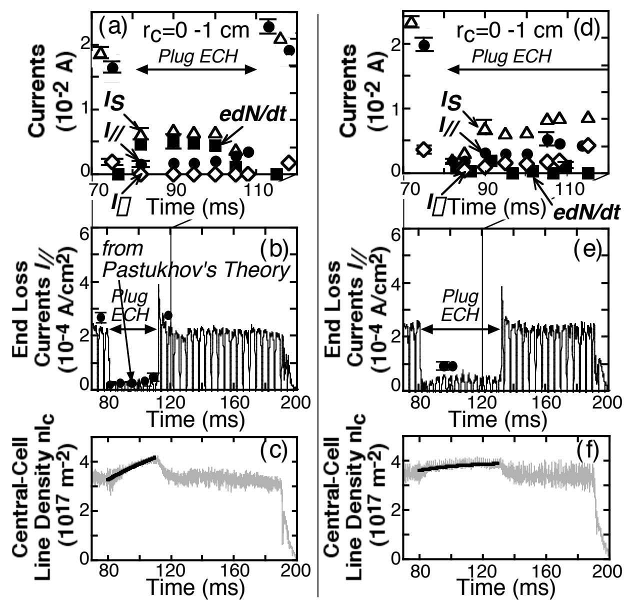

FIG. 4. Improved confinement in the hot-ion mode having a strong shear during ECH [Figs. 3(g)-3(k)] is analyzed from (a) a particle-balance equation; no appreciable transverse loss $I_\perp$, and consistently good agreement with (b) Pastukhov's predicted $I_{//}$ (filled circles) are found. (c) In fact, the particle-balance procedure demonstrates the good fit curve to the data in (c) [see also Fig. 3(a)] with the on-axis total particle-confinement time τ_{total}=75 ms (i.e. $\tau_{//}$=95 ms, and $\tau_\perp$>4$\tau_{//}$ at t=100 ms under a strong shear [Fig. 3(j)]); here, Pastukhov's ion-energy-confinement time τ_E=50 ms for the present medium height of ϕ_c=0.84 kV. On the other hand, poor confinement with a weak shear [Figs. 3(m)-3(q)] is accompanied by an appreciable $I_\perp$ in (d). This is consistent with an earlier saturation of nl_c in Fig. 3(l) as compared to its continuous rise in Fig. 3(a) during ECH. The particle-balance analyses totally demonstrates the good fit to the data in (f) [see also Fig. 3(l)] with τ_{total}=28 ms (i.e. $\tau_{//}$=45 ms, and $\tau_\perp$=90 ms for ϕ_c=0.48 kV at t=100 ms in (f) with a weak shear [Fig. 3(p)]). In (c) $T_{i\perp}$=5 keV at t=100 ms.

From these analyses, a *high potential production* and the *associated strong W_r or E_r shear formation* play essential roles in *improvements* of *both axial* and *transverse* plasma confinement *simultaneously*.

6. Observations of Temporal and Spatial Evolution of Turbulent Vortex Structures and Their Clear Up Due to the Radial Shear Formation

For identifying the spatial behavior and structure of turbulence signals [Fig. 3(b)] with a weak shear [Fig. 3(e)], in comparison to those [Fig. 3(g)] with a strong shear [Fig. 3(j)], contours of the central-cell soft x-ray brightness I_{sx} are observed in Figs. 5(b) and 5(a), respectively.

"Hot-colored" regions indicate higher plasma-pressure locations. One can find spatially and temporally varied turbulent vortex-like structures during a weaker shear period [Fig. 5(b)] in the absence of ECH [Figs. 3(b)-3(f)]. These turbulent structures are, however, going to clear up with ECH [Fig. 5(a)] together with simultaneous disappearance of the broad-band Fourier signal component [compare Figs. 3(b) with 3(g)] as well as a temperature rise [Fig. 5(a)]. A combination of x-ray data from the above-described detector array and another one having a separation of 135 degrees in the central midplane allows us to reconstruct a detailed vortex structure [Fig. 5(c)]. Its typical lifetime from formation to disappearance ranges around a hundred μs approximately with a rotational motion of an $E_r \times B_z$ drift. In Fig. 5(c), the center of the vortex-like structure appears around $r_c \approx 5$ cm and is faded at $r_c \approx 7$ cm into a detector noise level. Consequently, the existence of such vortex-like turbulent phenomena may provide a correlation with the appearance of the above-described additional transport $I_{\perp}$ with confinement degradation [Figs. 4(d), 4(e), and 5(b)] in the case with a weak shear, while such turbulence phenomena disappear and confinement is improved with a strong shear [Figs. 4(a), 4(b), and 5(a)]. In addition, similar spectra of x-ray signals to those of IES [Figs. 3(b) and 3(g)] under weak and strong shear conditions are shown in Figs. 5(d) and 5(e), respectively. From a common physics viewpoint, these researches by using easy controllability of the *radial electric shear* in open-ended mirror devices may provide an opportunity for exploring extended and generalized collaboration researches related to the physics-mechanism identification of H-mode pedestal and internal transport-barrier (ITB) formation [25].

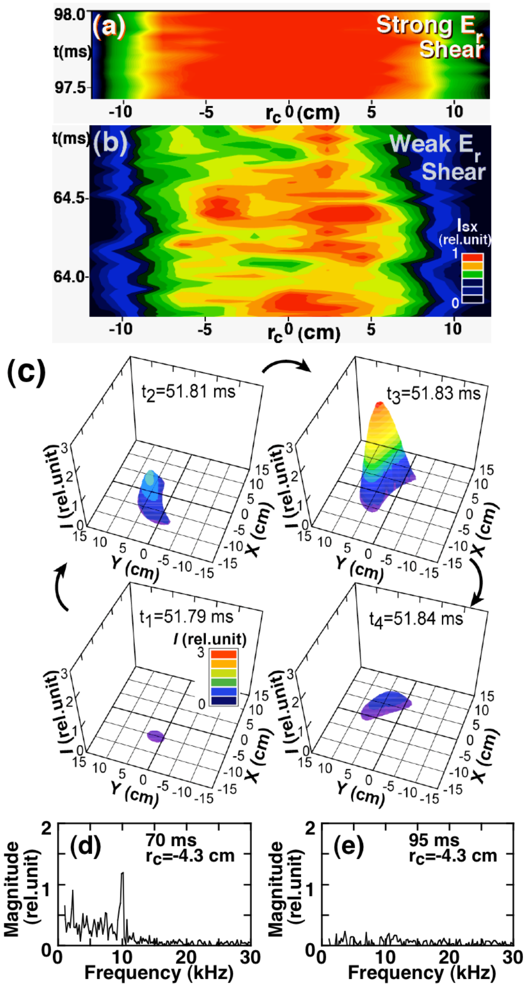

FIG. 5. Contours of central-cell x-ray brightness in the cases with (a) a strong and (b) a weak shear formation. "Hot-colored areas" show higher plasma-pressure locations ($I \propto n_e n_i T_e^{2.3}$). Vortex-like structures are found in (b). The temporal evolution of a vortex is exemplified in (c) by the use of our developed x-ray tomography systems. Fourier spectra of the x-ray signals also shows (d) similar continuous turbulent fluctuations along with peaked structures in the case with a weak shear [see also Fig. 3(b) for IES spectra], while (e) these are well suppressed with a strong shear [see Fig. 3(g)].

7. A Scaling of Potential Formation for Physics Mechanism Studies and Control of the Associated Radially Sheared Electric Fields Formation

For *constructing physics interpretations and control methods of such potential and the* *associated sheared E_r or W_r formation*, the validity of our proposed potential mechanisms [15] covering over (a) the high-potential and (b) hot-ion modes is extendedly tested in Fig. 6.

The theoretical essentials of the proposed consolidated theory [15] are briefly summarized as follows: The theoretical surfaces in Fig. 6 are calculated from the strong ECH theory (plateau formation) [6] in combination with generalized Pastukhov's theory on energy confinement [7]; that is, the dominant "electron losses" are made along lines of magnetic force compared to transverse losses, as employed in both theories [6,7]. Consequently, central-cell electrons having a temperature T_e [keV] and n_c [10^{18} m^{-3}] flow partially beyond ϕ_b [kV], and then into a plug region, where they contribute to an electron source term in the strong ECH theory [6]. The amount of these electrons overcoming ϕ_b is described in terms of the generalized Pastukhov theory. Therefore, the amount of source (target) electrons of plug ECH for plug potential formation is anticipated to closely relate to the electron energy (or particle) confinement time τ_{Ee} (i.e., the ratio of stored electrons to those lost beyond ϕ_b) estimated from Pastukhov's theory with ϕ_b and T_e (i.e., the use of the energy balance equation for the consolidation [15] of the two major theories). By using these physics bases, this consolidation procedure gives a general formula of $\phi_c = T_e[0.665(n_p/n_c)\exp(1.19\phi_b/T_e)]^{2/3} - \phi_b$, with $x = \phi_b/T_e = f^{-1}[2.01\times10^4 n_c^2 \ln\Lambda\, T_e^{-1/2} P_e^{-1}]$. Here, $f(x) = [x\exp(x)]/[(2/3)x + I(x^{-1})]$ with $I(x) \approx (1+x/2)/(1+x^2/4)$, the Coulomb logarithm $\ln\Lambda$, and total electron heating powers P_e [W m^{-3}] are employed for plotting the surfaces in Fig. 6.

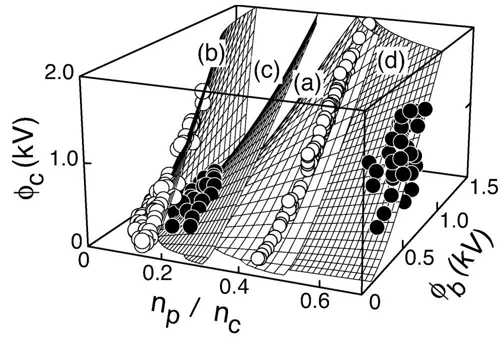

FIG. 6. The validity of theoretical surfaces for potential formation proposed in Ref. [15] covering (a) the high-potential and (b) hot-ion modes is extendedly investigated by using the advanced wider-ranged data for constructing potential physics interpretations and controlling potential enhanced E_r shear. Data well fit to the surfaces (c) and (d) for the modes of (b) and (a) with central ECH, respectively, along with (d) additional plug neutral beams.

In Fig. 6, as seen on the surfaces (c) and (d) with central ECH with (d) further additional plug neutral beams, the validity of the proposed theory is still confirmed under these auxiliary-heating conditions. Such good agreement between the data and the extension of our proposed consolidation encourages the validity and future extension of this scalable generalization.

8. A Scaling of Ion-Confining Potentials with Plasma Densities Ranging into Achieved $n_c \approx 10^{19}$m^{-3} with Ion Temperatures $T_i \sim$ keV and Ion-Confining Potentials ϕ_c > hundreds V

In the latest experimental series, high n_c oriented plasma operations with keV-ranged T_i and ϕ_c >hundreds V are carried out for constructing a scaling of ϕ_c with n_c and P_{ECH} in the hot-ion mode. From Fig. 7, a finding of preferable dependence of a weak decrease in ϕ_c with increasing n_c along with the recovery of ϕ_c with increasing P_{ECH} provides the future further extension of tandem-mirror properties into the n_c regime >10^{19} m^{-3} by the use of higher power ECH injections.

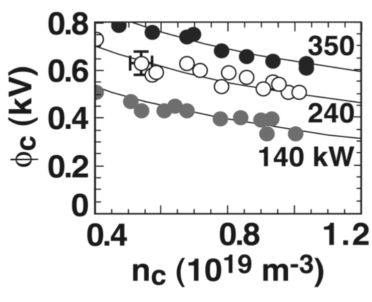

FIG. 7. In the hot-ion mode, a preferable scaling of a weak decrease in ϕ_c with increasing n_c along with the recovery of ϕ_c with increasing P_{ECH}, encourages the future further extension of tandem-mirror properties in the n_c regime >10^{19} m^{-3} due to higher power ECH installations.

9. Summary

In summary, following the Lyon IAEA Fusion Energy Conference [13], (1) *three-times progress in the formation of ϕ_c including a new record of 2.1 kV* is achieved in the hot-ion mode in comparison to ϕ_c attained 1992-2002 [13,14] (Fig. 2). (2) The advance in the potential formation leads to *a finding of remarkable effects of radially produced shear of electric fields* on *the suppression of vortex-like turbulent fluctuations* (Figs. 3, and 5), since the shear of E_r (more generally the dynamic vorticity W_r) is proportional to the heights of central-cell (ϕ_C) and plug potentials (ϕ_P). (3) The *clear-up of the turbulent vortex structures* due to a strong shear formation provides *plasma-confinement improvement in the transverse direction* (typically a few tens % of on-axis total τ_p with τ_E being improved into 0.1 with 0.05 s due to a strong shear; see Fig. 4). (4) These significant progresses on the basis of the high potential formation are made in line with the extension of our proposed *potential-formation physics scalings* [15] (Fig. 6). (5) A scaling of ϕ_c with n_c ranging into achieved $n_c \approx 10^{19}$ m^{-3} with $T_i \approx$ keV for ϕ_c>hundreds V is found to have preferable dependence of a weak decrease in ϕ_c with increasing n_c along with the recovery of ϕ_c with increasing P_{ECH} in the hot-ion mode (Fig. 7).

**Permanent Address*; Russian Research Center "Kurchatov Institute", Moscow, Russia.

[1] R. F. Post, Nucl. Fusion **27**, 1579 (1987); Trans. Fusion Sci. Tech. **43**, No. 1T, 195 (2003).
[2] D. D. Ryutov, *Review of Mirror Fusion*; in Proceedings of the International Conference on Plasma Physics, New Delhi, November 1989.
[3] M. Kwon *et al.*, Fusion Sci. Tech. **43**, 23 (2003); A. C. England *et al.*, ibid. **43**, No. 1T, 73 (2003).
[4] N. Hershkowitz, S. Miyoshi, and D. D. Ryutov, Nucl. Fusion **30**, 1761 (1990).
[5] S. Miyoshi *et al.*, Fizika Plazmy **23**, 781 (1997). [Plasma Phys. Reports **23**, 723 (1997).]
[6] R. H. Cohen, Phys. Fluids **26**, 2774 (1983).
[7] V. P. Pastukhov, Nucl. Fusion **14**, 3 (1974); R. H. Cohen *et al.*, Nucl. Fusion **18**, 1229 (1978); *ibid.* **19**, 1295 (1979); **19**, 1693 (1979).
[8] T. Cho *et al.,* Phys. Rev. Lett. **64**, 1373 (1990); Phys. Rev. **A 45**, 2532 (1992).
[9] T. Cho *et al.,* Nucl. Fusion **27**, 1421 (1987).
[10] T. Kariya *et al.,* Phys. Fluids **31**, 1815 (1988).
[11] T. Cho *et al.*, Nucl. Fusion **28**, 2185 (1988).
[12] T. Cho *et al.*, Nucl. Fusion **41**, 1161 (2001).
[13] T. Cho *et al.*, in Proceedings of 19th IAEA Fusion Energy Conf. (Lyon, 2002) IAEA-CN-94/EX/C1-4Ra.
[14] T. Cho *et al.*, Nucl. Fusion **43**, 293 (2003).
[15] T. Cho *et al.*, Phys. Rev. Lett. **86**, 4310 (2001).
[16] Y. Kiwamoto *et al.*, Phys. Plasmas **3**, 578 (1996).
[17] M. Ichimura *et al.*, Nucl. Fusion **39**, 1995 (1999).
[18] S. Tanaka *et al.*, Rev. Sci. Instrum. **70**, 979 (1999).
[19] M. Yoshida *et al.*, Rev. Sci. Instrum. **74**, 1909 (2003).
[20] K. Ishii *et al.*, Rev. Sci. Instrum. **60**, 3270 (1989).
[21] A. V. Timofeev, Review of Plasma Physics, Vol. 17, Consultants Bureau, New York (1992) 193-301.
[22] A. Mase *et al.*, Phys. Rev. Lett. **64**, 2281 (1990); Nucl. Fusion **31**, 1725 (1991).
[23] M. Hirata *et al.*, Nucl. Instrum. Methods **B66**, 479 (1992).
[24] I. Katanuma *et al.*, Nucl. Fusion **27**, 2041 (1987).
[25] Y. Kishimoto *et al.,* Nucl. Fusion **40**, 667 (2000), K. Itoh *et al.,* Plasma Phys. Control. Fusion **38**, 1 (1996). Various references being herein.